The Influence of Size and Morphology on Devolatilization of Biomass Particles

Anna Leth-Espensen[a], Tian Li[b], Peter Glarborg[a], Terese Løvås[b], Peter Arendt Jensen[a,*]

[a]*Department of Chemical and Biochemical Engineering, DTU - Technical University of Denmark, Søltofts Plads 229, 2800 Kgs. Lyngby*
[b]*Department of Energy and Process Engineering, NTNU - Norwegian University of Science and Technology, Kolbjørn Hejes vei 1b, 7491 Trondheim*

Abstract

This modeling study examines the effect of particle morphology on devolatilization of biomass particles at conditions relevant for suspension firing. A model, which can calculate devolatilization times and particle temperatures for both spherical and cylindrical particles is established, and modeling predictions are compared to experimental data from literature relevant for suspension firing with good consistency. The model predicts devolatilization times, which vary with more than two orders of magnitude in the particle size range (d_p = 0.2-3 mm) used in suspension firing. For the relevant gas temperature (T_g = 1300-1900 K) and density (ρ = 400-1000 kg/m^3) intervals, the devolatilization times vary with approximately a factor of two in both cases. Variations in moisture content primarily influence the time for onset of devolatilization, which may affect flame stability in suspension fired boilers. When modeling cylindrical biomass particles as spheres, the model further shows that it is

*Corresponding author
Email address: paj@kt.dtu.dk (Peter Arendt Jensen)

more accurate to keep the diameter of the cylinder than to adjust the radius to create a sphere with the same volume as the original cylinder. Finally, the present study includes an analysis of the relative effect on devolatilization time of relevant physical parameters for three particle sizes (d_p = 78.8μm, 400 μm, and 1560 μm). The analysis shows that a 30 % decrease in T_g increases devolatilization times by 82 % for small particles, but only by 11 % for larger particles.

Keywords: High heating rate, Devolatilization model, Particle Morphology, Biomass, Suspension Firing

---

1. Introduction

Increased interest in climate change has given rise to the use of biomass as a fuel in suspension firing units. Typically, suspension firing is conducted at high temperatures (> 1000 K), high heating rates (> 1000 K/s), and with small particles (d_p < 3 mm). Suspension firing has traditionally been done with coal, but due to the wanted reduction in net CO_2 emission, biomass has been introduced. Biomass particles differ from coal in size, shape, chemical composition and volatile fraction.[1–4] Models for coal particle combustion have often assumed an isothermal, zero dimensional (0D)[5] or one dimensional (1D) spherical geometry.[6] This approach is not suitable for elongated biomass particles, where the increased size results in internal temperature gradients, which cannot be neglected. Thus, with the transition from coal to biomass particles, modeling is required to include particles of different morphologies.[7–10] Compared to other morphologies, it is recommended by Trubetskaya[11, 12] to model biomass particles as cylinders in devolatiliza-

tion models. Typical aspect ratios ($AR = L/d_p$) for wood[13] are 2-3 and up to approximately 14 for herbaceous material.[11]

Experimental studies have illustrated the importance of representing particle gradients accurately. It is well known that thermal conversion of larger particles involves significant internal gradients. Larfeldt et al.[14] conducted experiments with large cylindrical particles (d_p = 50 mm, L = 300 mm) at moderate temperatures (973 K) in an electrically heated furnace, and Pilar Remacha et al.[15, 16] conducted experiments in a flat flame burner for medium sized, spherical particles (d_p = 3-15 mm) at T_g = 1380 K. Both of these experimental studies showed internal temperature gradients for large particles, and it was concluded that an isothermal 0D approach is not sufficient to describe devolatilization in larger particles. However, even for particle sizes relevant for suspension firing, it may be important to account for gradients. Bharadwaj et al.,[17] who conducted experiments in a downfired turbulent flow combustor at T_w = 1523 K, with a particle sieve size of 0.707-0.841 mm and aspect ratio 2-3, showed that both intraparticle heat and mass transfer are necessary to account for biomass particle devolatilization for particle sizes relevant for suspension firing. Based on model work, Johansen et al.[18] came to the same conclusion valid for all particle sizes under conditions relevant for suspension firing.

Bharadwaj et al. [17] further show that the aspect ratio decreases during devolatilization for both wood (red oak) and herbaceous material (alfalfa). The same conclusion was drawn for small softwood particles (sieve size 45-75 μm) by Lewis and Fletcher[19] in a flat flame burner at T_g = 1163-1433 K. Lu et al.[8] have looked at devolatilization of three different particle shapes (d_p

= 0.32-16 mm) in an entrained flow reactor and a single particle reactor and conclude that particle morphology influences devolatilization times and conversion rates due to the increase in surface to volume ratio for non-spherical particles. The corresponding model developed by Lu et al. indicates that particle morphology effects are important for particles exceeding 200-300 μm. Another devolatilization model describing both spherical particles and other geometries has been presented by Thunman et al.[20], and further developed by Ström and Thunman.[21] This model was validated against experimental data relevant for fluidized beds (d_p 10-40 mm, $T_g < 1123$ K, HR $\lesssim 10$ K/s). Gubba et al.[22] presented a model to account for intraparticle heat and mass transfer for co-firing with biomass, which can be implemented into CFD. However, their model was only validated with experimental data for large particles ($d_p = 9.5$ mm) at intermediate temperatures ($T_g = 1050$ K), so it is not necessarily applicable for the smaller particles utilized in suspension firing. To the knowledge of the authors, no model exists, which is validated against relevant experimental data and can adequately predict devolatilization times for small particles ($d_p < 3$ mm) at high temperatures and heating rates for different morphologies.

Even though particle devolatilization is described extensively in the literature, work that illustrates the effect of biomass particle morphology on particle ignition and devolatilization time for conditions relevant for suspension firing is scarce. The purpose of this paper is to further develop the model by Thunman, Ström, and coworkers[7, 21] to be relevant for suspension firing conditions, i.e. to be able to predict devolatilization behavior in smaller particle sizes at higher temperatures and heating rates. Firstly, this is done

by a modification to the model, so it now include sink and source terms for the energy required to heat water vapor and devolatilization gasses after reactions. Secondly, a new kinetic scheme incorporating both low and high heating rate Arrhenius kinetics is implemented, and submodels accounting for particle specific heat capacity and particle thermal conductivity are chosen according to the physico-chemical condition in a suspension firing unit. Thirdly, the model presented here is compared to experimental data from the literature in both the lower and the upper end of the suspension firing fuel size range. In this way, it is ensured that the improved model can describe all particle sizes in the relevant size range (d_p = 0.1-3 mm). Furthermore, this paper also illustrates the influence of key biomass properties' effect on devolatilization time. The effect of morphology, gas temperature, particle size, density, and moisture content on pyrolysis for three representative particle sizes (d_p = 79 µm, d_p = 0.8 mm, and d_p = 3 mm) has been investigated. The effect of these parameters on ignition time and flame stability in suspension fired units is discussed.

2. Method

The model adopted here, is originally by Thunman et al.[20] and Ström and Thunman.[21], and is developed for combusting particles in fluidized and fixed beds, i.e. for larger particles at lower temperatures than what is typically the case for suspension firing. In this paper the model is further developed to be able to describe single particle devolatilization under suspension firing conditions. Section 2.1 describes the structure of the model as it is put forward by Thunman, Ström and coworkers.[20, 21] Section 2.2

describes the new additions to the model, by presenting submodels and the kinetic scheme, chosen here, in order to expand the model to include devolatilization of smaller particles at suspension firing conditions.

2.1. Model Description

The model is constructed as a shell model, comparable in structure to an onion. It is a combination of a sharp interface model and a finite reaction zone model.[23] At $t = 0$ the particle primarily consists of moist wood, with infinitesimally thin outer layers of dry wood and char. As time progresses the outer regions of the particle are dried and devolatilized. Consequently, at time t, the particle consists of three concentric shells; an outer char shell, a middle dry shell, an inner moist shell. A sketch of the shell structure can be seen in figure 1.

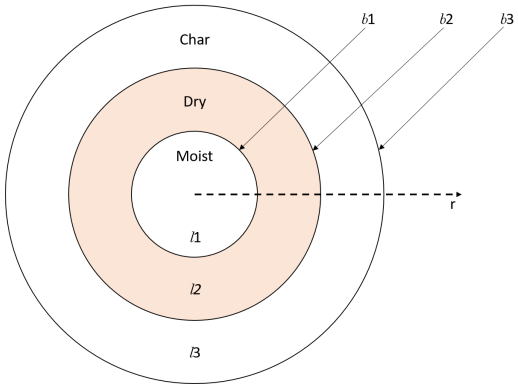

Figure 1: Sketch of shell structure. Adapted from Ström and Thunman.[21]

The evaporation of water happens at the interface between the moist and the dry zone. The devolatilization takes place in the dry zone, marked by the light peach colored area in figure 1. The heat balance for the outer shell includes external radiation and convection. The heat balances of the model

can be seen in equation 1 through 3, and the mass balances can be seen in equation 4 through 6. There are some slight modifications to the originally developed equations[21] marked in blue in equation 1 and 2. Q_{l2} is a source term for the energy required to heat the water released during evaporation and the energy required to heat the wood, from which the water has been released. The water vapor is heated from the release temperature, T_{b1}, to the temperature where it is transferred to the next shell, T_{b2}. The newly dried wood is heated from the release temperature, T_{b1}, to the temperature of the dry wood layer, T_{l2}. In the same fashion, Q_{l3} is a source term for the energy required to heat the gas released from the devolatilization, the energy required to heat the water released during evaporation (which has been transported trough the dry layer), and the energy to heat the char, in which the devolatilization has taken place. The volatiles and the water vapor are heated from the temperature at the shell boundary, T_{b2}, to the outer shell temperature, T_{b3}. The newly devolatilized wood (now char) is heated from the boundary temperature, T_{b2}, to the char layer temperature, T_{l3}.

$$\frac{dT_{l3}}{dt} = \frac{\alpha_{l3}}{V_{l3}}\left(A_{b3}\frac{dT}{dr}\Big|_{b3,l3} - A_{b2}\frac{dT}{dr}\Big|_{b2,l3}\right) + \frac{Q_{l3}}{C_p\rho V} \tag{1}$$

$$\frac{dT_{l2}}{dt} = \frac{\alpha_{l2}}{V_{l2}}\left(A_{b2}\frac{dT}{dr}\Big|_{b2,l2} - A_{b1}\frac{dT}{dr}\Big|_{b1,l2}\right) + \frac{Q_{l2}}{C_p\rho V} \tag{2}$$

$$\frac{dT_{l1}}{dt} = \frac{\alpha_{l1}A_{b1}}{V_{l1}}\frac{dT}{dr}\Big|_{b1,l1} \tag{3}$$

$$\frac{dm_{l3}}{dt} = \gamma\omega_{b2} \tag{4}$$

$$\frac{dm_{l2}}{dt} = \omega_{b1}/Y_{m,db} - \omega_{b2} \tag{5}$$

$$\frac{dm_{l1}}{dt} = -\omega_{b1}/Y_m \tag{6}$$

The boundaries (b) and shell layers (l) are numbered from the center outwards, so $l1$ is the wet layer, $b1$ is the boundary between wet and dry layer and so on. T_{li} is the temperature of layer i, α is the thermal diffusivity, V is the layer volume, A is the surface area, m is the layer mass, γ is the char yield, ω_{wb1} is the drying reaction rate, ω_{b2} is the pyrolysis reaction rate, and Y_m is the mass fraction of moisture. Boundary conditions for the heat balances are given in equation 7 through 9, assuming no heat accumulation at the boundaries.

$$hA_{b3}(T_g - T_{b3}) + \sum \epsilon_1 \sigma A_{b3}(T_w^4 - T_{b3}^4) = k_{p3} A_{b3} \frac{dT}{dr}\Big|_{b3,l3} \tag{7}$$

$$k_{l3} A_{b2} \frac{dT}{dr}\Big|_{b2,l3} = k_{l2} A_{b2} \frac{dT}{dr}\Big|_{b2,l2} + Q_{rxn,b2} \tag{8}$$

$$k_{l2} A_{b1} \frac{dT}{dr}\Big|_{b1,l2} F_{b1} = Q_{rxn,b1} \tag{9}$$

Here h is the heat transfer coefficient, ϵ is the emissivity, σ is the Stefan-Boltzmann constant, k is the thermal conductivity, and Q_{rxn} is a reaction heat flow. F_{b1} is an empirical parameter, which determines the ratio of the heat transferred to the drying front for water evaporation to that used to heat up the wet wood layer.

The model can describe devolatilization of both spherical and cylindrical particles. The sizes of the particles are characterized by the initial radius R for the sphere, and by both an initial radius, R, and a length, L, for the cylinder. The one-dimensional geometry of the sphere and an assumption of isotropy means that changes in size for the spherical particles can be characterized only by one time-dependent variable, the radius r. The cylindrical particles are two-dimensional, but can also be described using only one variable, r, plus the two constant parameters for the initial dimensions, R and

L. The length of the cylindrical particle is defined as a function of r as $l = L - 2(R - r)$. The implementation of the model is only made for cylinders with $L > 2R$. A sketch of the cylindrical particle can be seen in figure 2. By assuming that the reduction in diameter of a given shell equals the reduction in length, the number of variables needed to describe a cylinder can be reduced to one, assuming isotropy in the angular direction. This approach is a simplification of the end effects, but it allows for a simpler model. A model with a more detailed description of the end effects would have a devolatilization time higher than that for a sphere, but lower than the one predicted for a cylinder with the model presented here. As will be shown in section 4.2, the devolatilization time for a sphere and a cylinder with AR = 1.01 are practically the same, so describing the end effects at a higher computational cost is not relevant here. The same one variable approach to describe cylinders has been utilized by Porteiro et al.[24]. Yang et al.[25] have, using a two variable approach, described the end effects in more detail by allowing a faster release of volatiles at the cylinder ends. However, this approach typically yields greater computational costs, thus it has not been pursued here.

The model as presented by Thunman, Ström, and co-workers[20, 21] has been validated against experimental data with different morphologies (spheres, cylinders, and parallellipipeds), but only for large particles ($d_p >$ 9.5 mm) at moderate temperatures ($T_g <$ 1276 K). Thus, the original model has a verified capacity to predict biomass devolatilization under these conditions. However, larger particles at moderate temperatures are primarily heat transfer controlled. In contrast, the smaller particles utilized at suspension

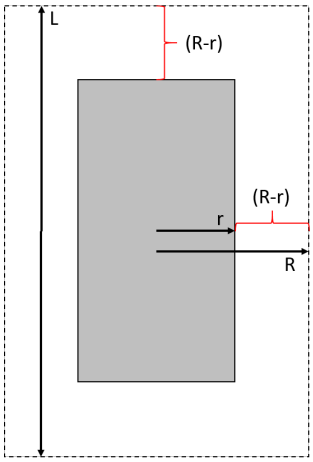

Figure 2: Sketch of geometry of cylindrical particle. Dashed line is initial outline of particle layer, solid grey figure is particle at $t > 0$.

firing will be kinetically controlled or in the transition region between kinetically controlled and heat transfer limited devolatilization. For the purpose of expanding the model to be able to predict devolatilization under suspension firing conditions, alternative submodels and expression for relevant physico-chemical properties are put forward in the subsequent section.

2.2. Model Input Parameters

An overview of the model parameters used in this study can be seen in table 1. The kinetic scheme builds on Arrhenius equations with different kinetic parameters for low and high heating rates, which can be seen in equation 10 through 12.

$$k_L = k_{L1} + k_{L2} + k_{L3} \tag{10}$$

$$k_{Lj} = A_{Lj}\, exp(-E_{a,Lj}/(RT)), \quad j = 1, 2, 3 \tag{11}$$

$$k_H = A_H\, exp(-E_{a,H}/(RT)) \tag{12}$$

The low heating rate kinetics are described by Wagenaar et al.[26] as three competing reactions and the high heating rate kinetics are described by a single first order reaction (SFOR) by Johansen et al.[27]. In this paper both low and high heating rate kinetics are treated as SFORs. The low heating rate kinetics are combined to a single rate constant as shown in equation 10, in order to ensure that the obtained char yield is not dependent on three competing reactions, relevant only for low temperatures. The transition from the low to the high heating rate should happen around 800 K.[28] It is here chosen to be linear, with the transition temperature interval between 750 and 950 K. An Arrhenius plot of the pyrolysis rates of different studies and the combined function utilized here can be seen in figure 3. Compared to the kinetics utilized here, the figure shows that at low temperatures the high heating rate kinetics predicts the reaction rate to be high, and at high temperatures the low heating rate kinetics also predicts the reaction rate to be high. The discrepancies between low and high heating rate kinetics also show that it is necessary to have different kinetic schemes when covering a large temperature span.

The specific heat capacities for wood and char are sensitive to temperature. Relations for C_p should not be extrapolated outside the interval, in which they have been derived without careful consideration. Comparison of some examples of C_p values for both dry wood and char can be seen in figure 4. Extrapolation of the linear C_p expressions result in extreme values for the specific heat capacities, especially at high temperatures. The only pair of related C_p values, which do not increase significantly by extrapolation to the relevant temperature interval are behold by Merrick et al.[37], hence they

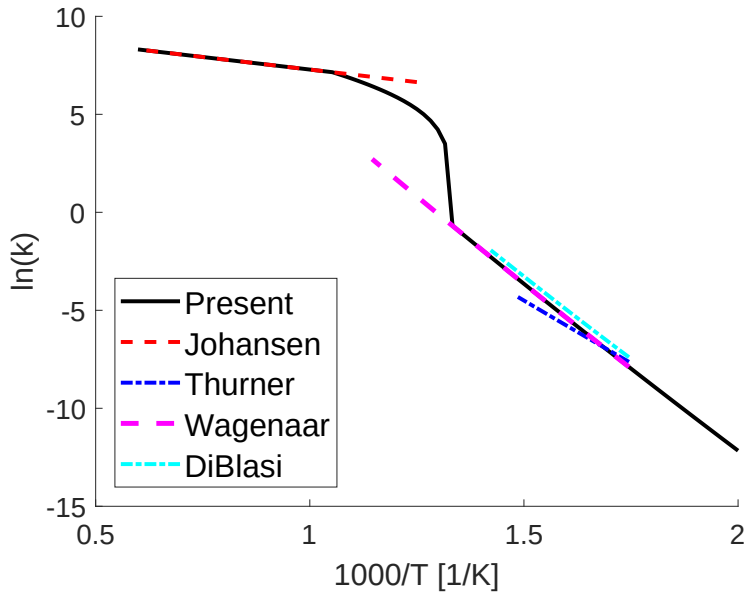

Figure 3: Arrhenius plot for kinetic scheme used in this model and literature models for high heating rate kinetics from Johansen et al.[27] and low heating rate kinetics from Wagenaar et al.[26], DiBlasi and Branca[42], and Thurner and Mann.[43]

have been chosen in the present work, even though they have originally been derived for coal. An expression for the specific heat capacity for wet wood is derived by TenWolde et al.[39], and is dependent on both moisture content and the C_p of dry wood. This expression is utilized here, using the expression for dry wood C_p developed by Merrick et al.

The change of enthalpy as a result of the desorption of water from a coal particle has been addressed by Callanan et al.[33] for multiple samples, all giving similar results. An average value of the provided data, 3.61 kJ/g, has been utilized here. The value is connected with some uncertainty as the data are obtained for coal particles, but the water content is low in the experiments investigated here (0-6 wt % wb) and in suspension firing units in

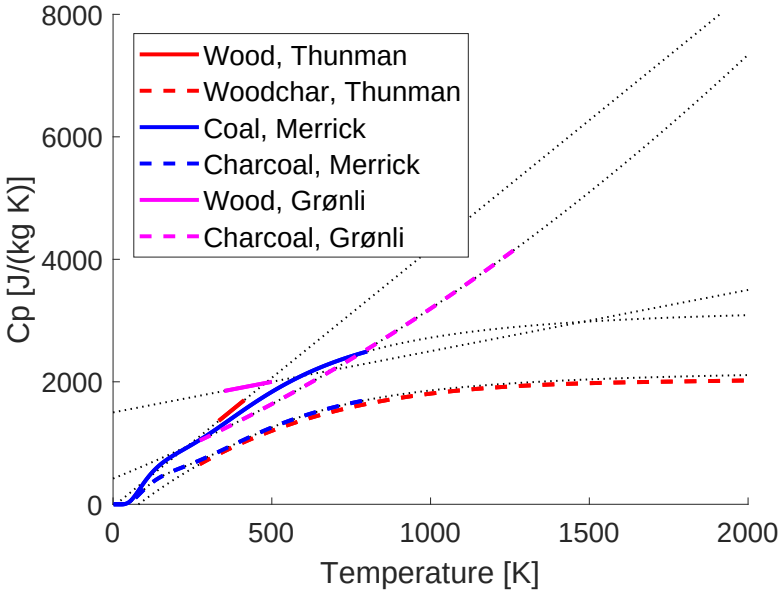

Figure 4: Comparison of C_p values from Thunman et al.[20], Merrick[37] and Grønli and Melaaen.[44] Black dotted lines are extrapolation of models.

general, meaning that the effect of any uncertainties are assumed insignificant. The change in enthalpy as a function of devolatilization reported in literature varies from being highly endothermic at 611 J/g wood[45] to being exothermic at -222 J/g.[46]. There seem to be little consensus in literature on any value for the heat of devolatilization, and most sources provide both exothermic and endothermic values.[21, 46] The discrepancy is likely due to differences in biomass, differences in operating conditions, and a different definition on how the devolatilization process is delimited. Most sources do, however, report the process to be slightly endothermic. In this work different heat of devolatilization values have been tested and compared to experimental results, and a value of 200 J/g has been chosen as it represents

experimental data well. The influence of changes in heat of devolatilization is tested in section 4.1.

The thermal conductivity of virgin wood is normally considered to be considerably higher than that of char,[40] but Brown[47] has shown that the thermal conductivity of char at elevated temperatures is twice that of virgin wood at ambient temperature, consequently both must be determined accurately. The thermal conductivity employed in this work builds on the correlation set forward by Koufopanos et al.[40]. They developed an empirical expression for the devolatilization of wood particles ($d_p = 20$ mm) under moderate temperatures ($T_g < 873$ K), that has been widely adopted, also for high heating rate experiments.[28, 48] No thermal conductivity correlation for wood at higher temperatures has been found in literature. Thermal conductivity for wet wood is approximately 15 % higher than that of dry wood according to table values for multiple wood species from the WoodHandbook[41], thus a 15 % increase in wet wood thermal conductivity has also been applied here.

The heat transfer coefficient, h, is an input parameter, which, regardless of particle shape, is estimated as described by Leth-Espensen et al.[29] h is calculated from the Nusselt number, which is not defined for free falling cylindrical particles in turbulent gas streams, hence a spherical correlation has been employed. Duan et al.[49] propose to relate the heat transfer coefficient to the drag coefficient and determine h in this way in order to avoid the dependence on the Nusselt number. Although possible, a limited number of experiments relating drag and heat transfer for cylindrical particles in free fall are available and therefore, a spherical assumption using the correlation for the Nusselt number is currently employed.

The model predicts both the temperature of each of the three particle boundaries (moist wood, dry wood, and char) as shown in figure 5 and the temperature and mass of each of the three particle layers. In figure 5a the mass of each of the three layers and the total mass of the particle can be seen. It can be seen that the mass of the moist layer decreases over time, whereas the dry wood layer first increase as water is evaporated, and subsequently decreases as the wood is devolatilized. The char layer steadily increases until it reaches the specified char yield. The total mass of the particle decreases over time until only char is left. Figure 5b shows the temperature on the outer surface of each shell. The surface temperature is thus identical to the char boundary temperature, T_{b3}, in this figure. The dry layer temperature is increasing as the particle is heated, but stagnates during devolatilization as the process is endothermic. The moist boundary temperatures, T_{b1}, is close to the center temperature as the entire moist layer is slowly heated to the boiling temperature, and remains at T_{boil} during water evaporation. The moist layer temperature, T_{l1}, is the average temperature in the moist layer and is plotted in the remainder of this paper as a substitute for the particle center temperature, which is not obtained in this model.

3. Model Validation

This section covers the validation of the model with experimental data relevant for suspension firing for both spherical and cylindrical particles. The model is validated against data sets involving particles in the diameter range 78.8 μm to 9.5 mm. The degree of devolatilization in the following graphs is release of volatiles excluding the water present in the particle.

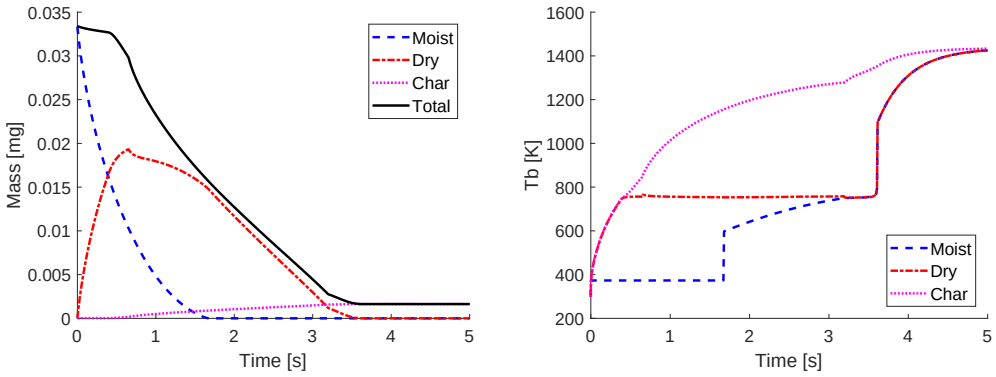

(a) (b)

Figure 5: Example of mass and temperature profiles provided by the model. Here for a particle with AR = 2, ρ = 700 kg/m^3, T_g = 1600 K, T_w = 1400 K, moisture content = 4 wt% wb, and r_{ini} = 1560 µm.

3.1. Summation of Model Validation

The model is validated for particles in the parameter intervals give in table 2. The model is validated in the entire size interval relevant for suspension firing, also the main part of the parameter ranges for moisture content, gas temperature, and density are covered. For the aspect ratio the relevant range for wood particles is covered.

3.2. Particles with d_p = 78.8 µm

Experiments with small wood particles have been performed by Johansen et al.[27, 50]. The experiments were conducted in a laminar entrained flow reactor with fuel feed rates low enough to create single particle conditions. The maximum gas temperatures were 1405-1667 K, the heating rate was in the order 10^5 K/s, and the residence time from 0-100 ms. The applied experimental parameters are given in table 3. The char yield is estimated using the

method described by Leth-Espensen et al.[29], and the length is estimated based on recommendations from Masche et al.[13]. Figure 6 shows the comparison between experimental results for pine wood and model predictions for $T_g = 1405$ K and $T_g = 1667$ K. Also experimental data from four other biomass samples devolatilized under the same conditions in the same equipment have been included in the figure. The fuel types (pine, mischanthus, doped pine, leached mischanthus) all behave very similarly, and the major difference is the char yield. The four additional fuel types aid in describing the very rapid heating of particles of this size, where data points are scarce. The devolatilization of the particles happen within the first 20 ms in the reactor.

The figure shows consistency between experimental and model data. The small particles are rapidly devolatilized after an initial, short heating period. The relatively small diameter of the particles entails that these particles mimic isothermal particles. For an isothermal particle a short heating period would also be expected, before a rapid devolatilization commences.

3.3. Particles with $d_p = \sim 3$ mm

Experiments with 3 mm particles have been conducted by Lu et al.[52] in a single particle combustor. The particles are fixed on a small wire, located in a hot fluegas above a flame, and the devolatilization time is determined by video registration. The particles have been carved to near-spherical shapes, and are modeled as such. The temperature in the gas phase is $T_g = 1487$ K, and the initial heating rates are in the order $10^2 - 10^3$ K/s. The experimental data are given in table 4. Figure 7 shows the comparison of the devolatilization times for 3 mm spherical particles of different density for pine and beech

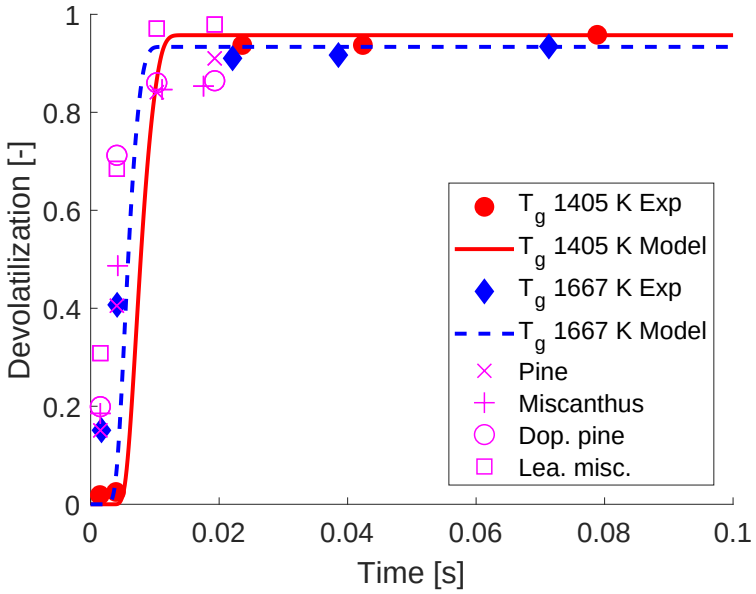

Figure 6: Comparison of model predictions to literature data for pine from Johansen et al.[27]. $d_p = 78.8$ µm, AR = 2, $\rho = 591$ kg/m^3, moisture content ≈ 0. Additional input parameters to the model are given in table 3. The pink data points are for four biomass types (pine, miscanthus, KCl doped pine, leached miscanthus) devolatilized under identical conditions as reported by Johansen et al.[50]

wood. The wood type is indirectly a parameter in the model as the char yield varies depending on the wood sort. The char yield was estimated using the method described by Leth-Espensen et al.[29] The particles also vary slightly in diameter.

The measured pyrolysis time increases with increasing density in the experimental dataset in agreement with the model predictions. The model is particularly accurate for the beech samples, but for both wood species, the trend is captured well. Complete devolatilization of the 3 mm particles was obtained after 3.5 to 6.5 seconds.

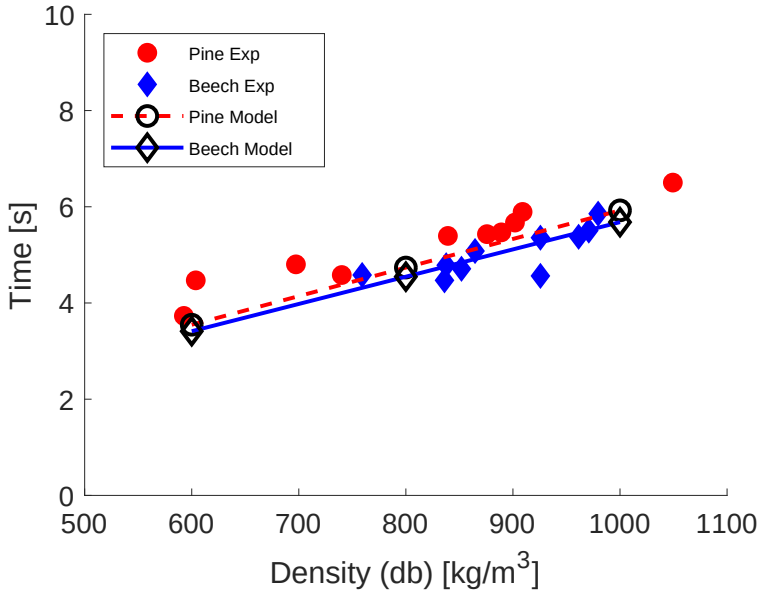

Figure 7: Comparison of devolatilization time for 3 mm spherical particles of different density. Experimental data from Lu et al.[52] $T_g = 1487$ K, $T_w = 1187$ K (estimated value), moisture content = 5.5 wt % wb. Additional input parameters to the model are given in table 4.

3.4. Particles with $d_p = 9.5$ mm

Lu[53] has conducted experiments with spherical and cylindrical particles, both 9.5 mm in diameter, and the cylinders have a length of 38 mm. The experiments were conducted in a single particle combustor, and each experiment was repeated three to four times. For the spherical particles the settings were the same in all three repetitions. For the cylindrical particles the settings were the same except that the thermocouple measuring the center temperature was placed radially in experiment 1 and 2, and axially in experiment 3 and 4. The maximum gas temperature in the experiments was 1276 K, and the initial heating rate was in the order of $10^1 - 10^2$ K/s. The

experimental data are given in table 5.

The temperatures in the devolatilization experiment for the cylindrical particle have previously been compared to the model presented by Ström and Thunman[21], and these results are also included in figure 9b. The two models show similar results for the temperatures of these large particles. Ström and Thunman have, however, not reported the degree of devolatilization related to the temperature measurements, and the comparison of experimental data from devolatilization of spherical and cylindrical poplar particles at identical conditions in the same set-up have not been made either. The latter is the reason of interest for this study.

Figure 8a and figure 8b show the degree of devolatilization and the temperature measurements for the spherical particles. The devolatilization of the spherical 9.5 mm particles take approximately 35 seconds. Figure 9a and figure 9b show the degree of devolatilization and the temperature measurements for the cylindrical particles. For the 9.5 mm cylindrical particle the devolatilization time is approximately 50 s. For both the spherical and the cylindrical particles, the thermocouple influences the devolatilization. The conducting material of a thermocouple may cause measurement errors of up to 300 K for millimeter-sized particles in high temperatures (T_g = 1653 K).[15] It is especially critical for the center temperatures, which are thus likely measured above the temperature in an unaffected particle.

The devolatilization is predicted well by the model both for the spherical and cylindrical particles, albeit the model prediction is slightly faster than the experimental results. The surface temperature is also predicted well. The center temperature is predicted reasonably by the model. The parti-

cle center temperatures measured experimentally are likely an overestimate as they have been measured with a thermocouple, which entails the shortcomings described above. The particle center temperatures predicted by the model are likely an underestimate, as e.g., the moist layer temperature is defined as equal to T_{boil} until all water is evaporated. However, the stepwise temperature profile for drying is also observed by Pilar Remacha et al.[16] during drying of alumina particles in a flat flame burner at 1573 K, so the assumption is expected to be reasonable. The combination of overprediction of experimental temperatures and underprediction of model temperatures is the reason for the small discrepancies seen in figure 8b and 9b. The results of the quardruplicate experiments also show that the experimental variation is considerable.

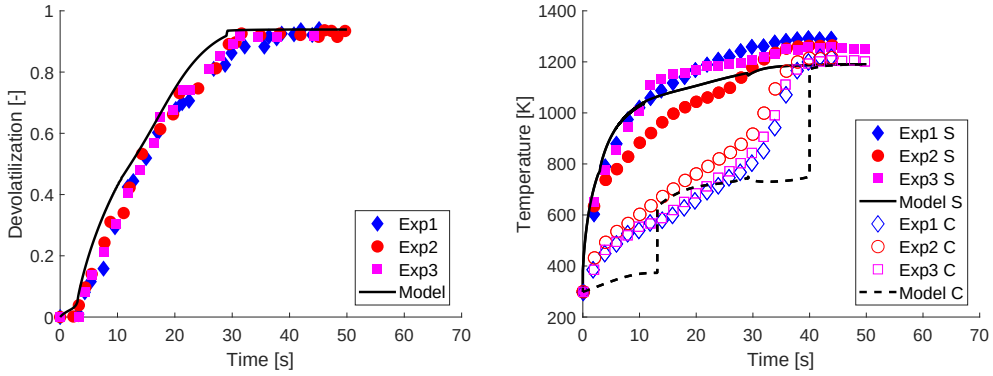

(a) (b)

Figure 8: Comparison of model to experimental data of spherical particles from Lu et al.[53] d_p = 9.5mm, ρ = 580 kg/m^3, T_g = 1276 K, T_w = 1176 K (estimated value), moisture content = 6 wt% wb. Additional input parameters to the model are given in table 5. The small fluctuation in the graphs around t = 30 s is due to the change in kinetic scheme. S = surface temperature, C = Center temperature.

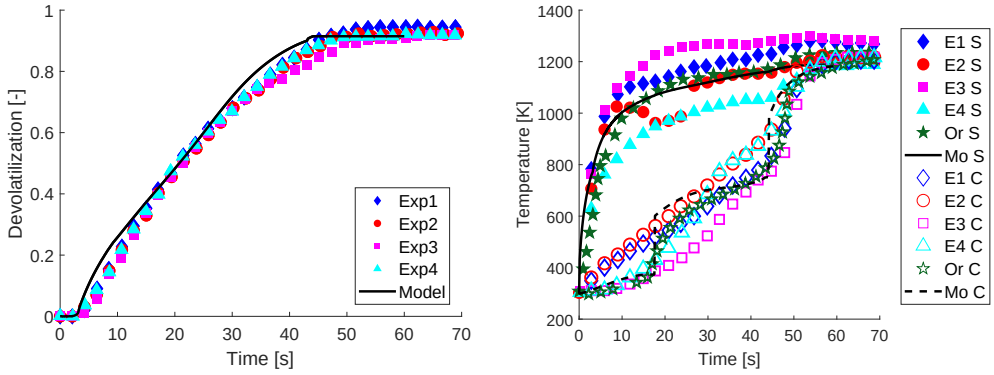

(a) (b)

Figure 9: Cylindrical particles modeled with current model (Mo) compared to model results from Ström and Thunman (Or) and experimental data from Lu et al.[53] d_p = 9.5 mm, AR = 4, $\rho = 580$ kg/m^3, $T_g = 1276$ K, $T_w = 1176$ K, moisture content = 6 wt% wb. Input parameters to the model are given in table 5. S = surface temperature, C = Center temperature.

4. Model predictions

4.1. Sensitivity Analysis

To investigate the influence of the material value properties and some particle and boundary conditions a sensitivity analysis with respect to devolatilization time has been conducted. The influence of particle properties and devolatilization conditions is tested for three different particle sizes (d_p = 79 µm, 800 µm, and 3.12 mm), since the influence of the model parameters varies depending on size. The other applied particle parameters can be seen in table 6.

The smaller particles are kinetically controlled, whereas the devolatilization process for the larger particles is limited by heat transfer mechanisms. In table 7 the effect of decreasing and increasing a number of parameters by

30 % can be seen. It can be concluded that radius, density, and gas temperature are important parameters, when determining the devolatilization time. For the first two the impact is highest for the smaller particles, whereas the impact of T_g is most pronounced for the larger particles. The influence of particle heat conductivity, k_p, is considerable for larger particles, whereas the effect for smaller particles seems to be less pronounced in good agreement with the larger particles being heat transfer controlled. To check the effect of the kinetic scheme, the Arrhenius reaction rates, k_L and k_H, have both simultaneously been increased and decreased by 30 %. The choice of rate constants mainly influences the smaller particles' devolatilization times, as they are primarily controlled by the kinetics of the devolatilization.

4.2. Parameter Analysis

A parameter analysis was performed to study the effect of particle properties and local conditions on the devolatilization time and further illustrate the influence on the devolatilization process. The analysis is done for a cylindrical particle ($d_p = 1.51$ mm, AR = 5) as baseline particle. Its characteristics are given in table 8. For each input parameter a low, an average and a high value is chosen to cover the parameter span relevant for suspension firing. The effect of changes in aspect ratio (for particles with the same radius), aspect ratio (for particles with the same volume), radius (for particles with the same aspect ratio), density, moisture content, and gas temperature is shown in figure 10.

The influence of aspect ratio on devolatilization time is shown both for particles with the same radius and for particles with the same volume in figure 10a and figure 10b, respectively. Comparing the figures shows that

in the case of identical radii, the effects on devolatilization times are minor, especially for AR > 5, whereas for particles with the same volume the effects of AR on devolatilization times are greater. Thus from a modeling perspective, even if it is chosen to model biomass particles as spherical, using the true diameter as an input parameter yields a better result with respect to estimating the devolatilization time. However, this approach might lead to other complications, e.g. in CFD, where a true representation of the entire mass of particles is necessary, and where the drag effect would also need to be accounted for.[54]

Comparing the effect of changes in radius in figure 10c to the model parameters in the remaining subfigures show that the particle size is an important input parameter to specify as accurately as possible. The devolatilization time varies with approximately two magnitudes within the particle size interval relevant for suspension firing. The particle size influences both the starting time for devolatilization, the amount of volatiles released and the total devolatilization time.

Another parameter, which has a considerable influence, especially on the onset of devolatilization, is the gas temperature as seen in figure 10d. The lower the gas temperature, the longer it takes to dry out the particle and heat it to a temperature where the devolatilization is initiated. The high, local temperature near the burner quarl ensures a fast onset of devolatilization, which improves ignition and flame stability.

The influence of the particle density can be seen in figure 10e. The density for the particles varies both dependent on biomass type and pelletilization procedure. The changes in density affects both the onset time for the de-

volatilization and the duration of it.

Compared to the other parameters, the moisture content seen in figure 10f has a smaller effect on total devolatilization time, but it has a strong influence on the onset of volatile release, and may consequently influence flame ignition. The moisture content in suspension fired units rarely exceed 10 wt% wb as the pelletilization and milling processes result in partly dried particles.

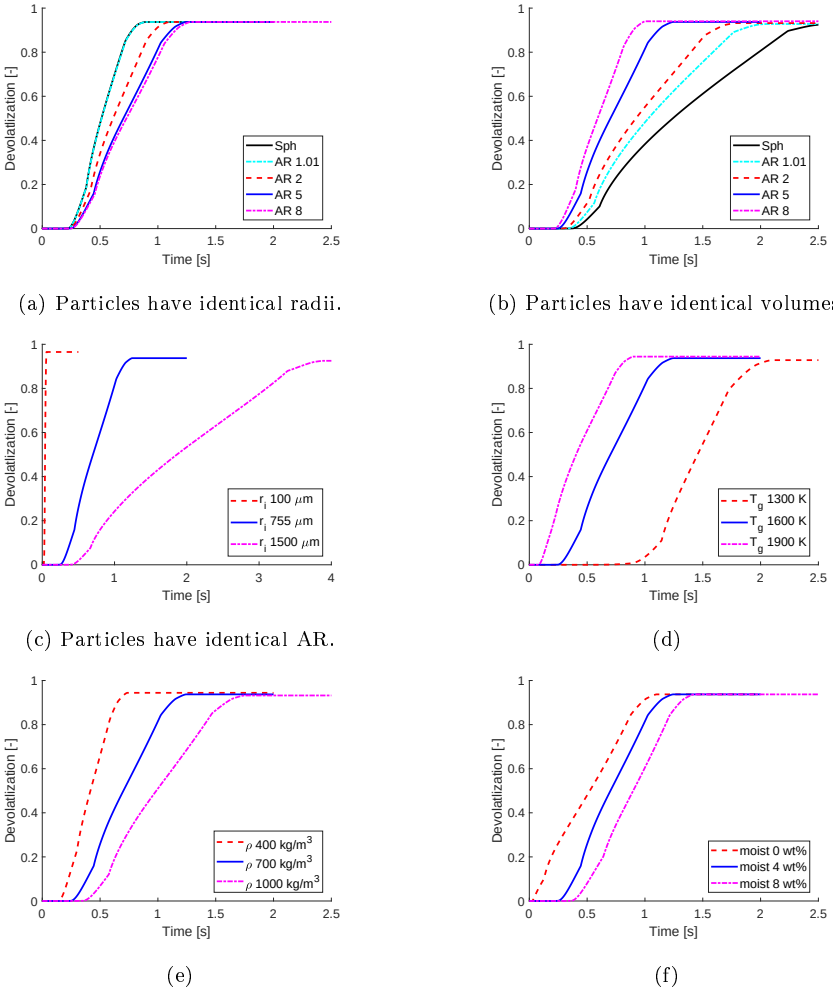

(a) Particles have identical radii.

(b) Particles have identical volumes.

(c) Particles have identical AR.

(d)

(e)

(f)

Figure 10: Parameter analysis for relevant particle properties and boundary conditions. Baseline simulation properties include AR = 5, T_g = 1600 K, R = 0.755 mm, ρ = 700 kg/m^3, moisture content = 4 wt % wb, represented by the blue solid lines.

5. Conclusion

The presented wood particle devolatilization model can describe biomass particles as both spherical and cylindrical and include end effects. The model

fits experimental data from the literature well for particle sizes (d_p = 79 μm to 9.5 mm) and in the temperature range (1276-1667 K), which is relevant for suspension firing.

The model results show that if a cylindrical particle should be approximated by the geometrically simpler sphere, the diameter of the cylinder is a better approximation for a particle size than the same volume approach, where the diameter is determined as the diameter of a sphere with the same volume as the cylinder.

The model further predicts devolatilization times to vary approximately two magnitudes for the particle sizes (d_p = 0.2-3 mm) utilized in suspension fired boilers, affecting both burnout and flame stability. Other parameters of importance for devolatilization time are particle density, and local gas temperature. Of minor importance for the final devolatilization time is moisture content, within the span relevant for pelletilized biomass. The moisture content, however, influences the onset of volatile release substantially.

A sensitivity analysis performed for three different particle sizes (d_p = 79 μm, 800 μm, and 3.12 mm) shows that the importance of determining the input parameters to the model correctly varies greatly with particle size. The most significant parameters are radius, density, and T_g. E.g. for T_g the devolatilization time increases with 82 % for particles with diameter 79 μm, whereas it only increases with 11 % for particles with radius 3.12 mm, when T_g is decreased by 30 %.

6. Acknowledgements

The authors thank Ørsted A/S, Rambøll A/S and Burmeister & Wain Scandinavian Contractors A/S for financial and advisory support. The Nordic 5 Tech Alliance (N5T) is also thanked for financial support. The authors also thank Henrik Ström from Chalmers University of Technology for assisting with the model development.

Nomenclature

Abbreviations

AR	aspect ratio
C	center
CFD	Computational Fluid Dynamics
cyl	cylinder
daf	dry ash free basis
db	dry basis
S	surface
SFOR	single first order reaction
sph	sphere
wt	weight

Greek Characters

α	thermal diffusivity	$[m^2/s]$
ϵ	emissivity coefficient	[-]
γ	char yield	[-]
ω	reaction rate	[kg/s]

ρ	density	$[kg/m^3]$

Roman Characters

ΔH	Enthalpy	$[J/kg]$
$\mathcal{L}$	Latent heat	$[J/kg]$
A	Surface area	$[m^2]$
C_p	specific heat capacity	$[J/(kg\cdot\ K)]$
d_p	diameter	$[mm/\mu m]$
F	Evaporation heat function	[]
h	convective heat transfer coefficient	$[J/(s{\cdot}m^2{\cdot}K)]$
k	reaction rate	$[s^{-1}]$
k	thermal conductivity	$[J/(s{\cdot}m{\cdot}K)]$
L	initial particle length	[mm or μm]
l	particle length	[mm or μm]
m	mass	[kg]
Nu	Nusselt Number	
Q	Heat flow	[J/s]
R	initial particle radius	[mm or μm]
r	particle radius	[mm or μm]
T	Temperature	[K]
t	time	[s]
V	Volume	$[m^3]$
Y	mass fraction	[-]
y	moisture content	[wt fraction db]

Sub- and Superscripts

p	particle
b	boundary
boil	boiling
desorp	desorption
devo	devolatilization
g	gas
H	high
j	integer
L	low
l	layer
m	moisture
rxn	reaction
w	radiation temperature

References

[1] M. A. Saeed, G. E. Andrews, H. N. Phylaktou, B. M. Gibbs, Global kinetics of the rate of volatile release from biomasses in comparison to coal, Fuel 181 (2016) 347–357. doi:10.1016/j.fuel.2016.04.123.
URL http://dx.doi.org/10.1016/j.fuel.2016.04.123

[2] D. Gera, M. P. Mathur, M. C. Freeman, A. Robinson, Effect of large aspect ratio of biomass particles on carbon burnout in a utility boiler, Energy Fuels 16 (6) (2002) 1523–1532. doi:10.1021/ef0200931.

[3] D. E. Priyanto, S. Ueno, K. Hashida, H. Kasai, Energy-efficient milling method for woody biomass, Adv. Powder Technol. 28 (7) (2017)

1660–1667. doi:10.1016/j.apt.2017.04.005.
URL https://linkinghub.elsevier.com/retrieve/pii/S0921883117301590

[4] M. Mandø, L. Rosendahl, C. Yin, H. Sørensen, Pulverized straw combustion in a low-NOx multifuel burner: Modeling the transition from coal to straw, Fuel 89 (10) (2010) 3051–3062. doi:10.1016/j.fuel.2010.05.016.

[5] H. Jüntgen, K. H. van Heek, An Update of German Non-isothermal Coal Pyrolysis Work, Fuel Process. Technol. 2 (1979) 261–293.

[6] P. K. Agarwal, W. E. Genetti, Y. Y. Lee, Model for devolatilization of coal particles in fluidized beds, Fuel 63 (8) (1984) 1157–1165. doi:10.1016/0016-2361(84)90205-9.

[7] H. Thunman, F. Niklasson, F. Johnsson, B. Leckner, Composition of volatile gases and thermochemical properties of wood for modeling of fixed or fluidized beds, Energy and Fuels 15 (6) (2001) 1488–1497. doi:10.1021/ef010097q.

[8] H. Lu, E. Ip, J. Scott, P. Foster, M. Vickers, L. L. Baxter, Effects of particle shape and size on devolatilization of biomass particle, Fuel 89 (5) (2010) 1156–1168. doi:10.1016/j.fuel.2008.10.023.
URL http://dx.doi.org/10.1016/j.fuel.2008.10.023

[9] N. Sousa, J. L. T. Azevedo, Model simplifications on biomass particle combustion, Fuel 184 (2016) 948–956.

[10] J. J. Saastamoinen, Simplified model for calculation of devolatilization in fluidized beds, Fuel 85 (17-18) (2006) 2388–2395. doi:10.1016/j.fuel.2006.04.019.

[11] A. Trubetskaya, G. Beckmann, J. Wadenbäck, J. K. Holm, S. P. Velaga, R. Weber, One way of representing the size and shape of biomass particles in combustion modeling, Fuel 206 (2017) 675–683. doi:10.1016/j.fuel.2017.06.052.
URL http://dx.doi.org/10.1016/j.fuel.2017.06.052

[12] A. Trubetskaya, Fast pyrolysis of biomass at high temperatures, Ph.D. thesis, Department og Chemical amd Biochemical Engineering, DTU (2016).

[13] M. Masche, M. Puig-Arnavat, J. Wadenbäck, S. Clausen, P. A. Jensen, J. Ahrenfeldt, U. B. Henriksen, Wood pellet milling tests in a suspension-fired power plant, Fuel Processing Technology 173 (February) (2018) 89–102. doi:10.1016/j.fuproc.2018.01.009.
URL https://doi.org/10.1016/j.fuproc.2018.01.009

[14] J. Larfeldt, B. Leckner, M. C. Melaaen, Modelling and measurements of the pyrolysis of large wood particles, Fuel 79 (2000) 1637–1643.

[15] M. P. Remacha, S. Jiménez, J. Ballester, Devolatilization of millimeter-sized biomass particles at high temperatures and heating rates. Part 1: Experimental methods and results, Fuel 234 (July) (2018) 757–769. doi:10.1016/j.fuel.2018.07.016.
URL https://doi.org/10.1016/j.fuel.2018.07.016

[16] M. P. Remacha, S. Jiménez, J. Ballester, Devolatilization of millimeter-sized biomass particles at high temperatures and heating rates. Part 2: Modeling and validation for thermally-thin and -thick regimes, Fuel

234 (February) (2018) 707–722. doi:10.1016/j.fuel.2018.07.017.
URL https://doi.org/10.1016/j.fuel.2018.07.017

[17] A. Bharadwaj, L. L. Baxter, A. L. Robinson, Effects of Intraparticle Heat and Mass Transfer on Biomass Devolatilization : Experimental Results and, Energy and Fuels 18 (4) (2004) 1021–1031.

[18] J. M. Johansen, P. A. Jensen, P. Glarborg, M. Mancini, R. Weber, R. E. Mitchell, Extension of apparent devolatilization kinetics from thermally thin to thermally thick particles in zero dimensions for woody biomass, Energy 95 (2016) 279–290. doi:10.1016/j.energy.2015.11.025.
URL http://dx.doi.org/10.1016/j.energy.2015.11.025

[19] A. D. Lewis, T. H. Fletcher, Prediction of Sawdust Pyrolysis Yields from a Flat-Flame Burner Using the CPD Model, Energy and Fuels 27 (2013) 942–953.

[20] H. Thunman, B. Leckner, F. Niklasson, F. Johnsson, Combustion of wood particles - A particle model for Eulerian calculations, Combustion and Flame 129 (1-2) (2002) 30–46. doi:10.1016/S0010-2180(01)00371-6.

[21] H. Ström, H. Thunman, CFD simulations of biofuel bed conversion: A submodel for the drying and devolatilization of thermally thick wood particles, Combustion and Flame 160 (2) (2013) 417–431. doi:10.1016/j.combustflame.2012.10.005.

[22] S. R. Gubba, L. Ma, M. Pourkashanian, A. Williams, Influence of particle shape and internal thermal gradients of biomass particles on pul-

verised coal/biomass co-fired flames, Fuel Processing Technology 92 (11) (2011) 2185–2195. doi:10.1016/j.fuproc.2011.07.003.

[23] A. Gómez-Barea, B. Leckner, A. L. Villanueva Perales, M. Campoy, Analytical solutions of sharp interface models with nth order kinetics. Application to char conversion, Chem. Eng. J. 183 (2012) 408–421. doi:10.1016/j.cej.2011.12.053.
URL http://dx.doi.org/10.1016/j.cej.2011.12.053

[24] J. Porteiro, J. L. Míguez, E. Granada, J. C. Moran, Mathematical modelling of the combustion of a single wood particle, Fuel Processing Technology 87 (2) (2006) 169–175. doi:10.1016/j.fuproc.2005.08.012.

[25] Y. B. Yang, V. N. Sharifi, J. Swithenbank, L. Ma, L. I, J. M. Jones, M. Pourkashanian, A. Williams, L. I. Darvell, Combustion of a Single Particle of Biomass Combustion of a Single Particle of Biomass, Energy 22 (8) (2008) 306–316. doi:10.1021/ef700305r.

[26] B. M. Wagenaar, W. Prins, W. P. M. van Swaaij, Flash Pyrolysis Kinetics of Pine Wood, Fuel Process. Technol. 36 (1993) 291–298.

[27] J. M. Johansen, R. Gadsbøll, J. Thomsen, P. A. Jensen, P. Glarborg, P. Ek, N. D. Martini, M. Mancini, R. Weber, R. E. Mitchell, Devolatilization kinetics of woody biomass at short residence times and high heating rates and peak temperatures, Applied Energy 162 (2016) 245–256. doi:10.1016/j.apenergy.2015.09.091.
URL http://dx.doi.org/10.1016/j.apenergy.2015.09.091

[28] J. M. Johansen, Power Plant Burners for Bio-Dust Combustion, Ph.D. thesis, DTU (2015).

[29] A. Leth-Espensen, P. Glarborg, P. A. Jensen, Predicting Biomass Char Yield from High Heating Rate Devolatilization Using Chemometrics, Energy and Fuels 32 (9) (2018) 9572–9580. doi:10.1021/acs.energyfuels.8b02073.

[30] Ražnjević, Handbook of Thermodynamic tables and charts, Hemisphere Publishing Corporation, 1976.

[31] M. Grønli, A theoretical and experimental study of the thermal degredation of biomass, Ph.D. thesis, NTNU (1996).

[32] Engineering toolbox - latent heat of vaporization of fluids - alcohol, ether, nitrogen, water and more, https://www.engineeringtoolbox.com/fluids-evaporation-latent-heat-d_147.html, accessed: 2019-03-06 (2003).

[33] J. E. Callanan, B. J. Filla, K. M. McDermott, S. A. Sullivan, Enthalpies of desorption of water from coal surfaces, Proceedings of ACS Symposium, Devision of Fuel Chemistry, Denver, CO, 185-192 (1987).

[34] J. A. Havens, J. R. Welker, C. M. Sliepcevich, Pyrolysis of Wood: A thermoanalytical Study, J. Fire & Flammability 2 (1971) 321–333.

[35] J. Chase, M.W., "Thermophysical Properties of Fluid Systems" in NIST Chemistry WebBook, NIST Standard Reference Database Number 69, National Institute of Standards and Technology, Gaithersburg MD,

20899, 1998.
URL http://webbook.nist.gov

[36] J. Chase, M.W., "Water" in NIST Chemistry WebBook, NIST Standard Reference Database Number 69, NIST-JANAF Thermochemical Tables, Fourth Edition, J. Phys. Chem. Ref. Data, Monograph 9, National Institute of Standards and Technology, Gaithersburg MD, 20899, 1998.
URL http://webbook.nist.gov

[37] D. Merrick, Mathematical models of the thermal decomposition of coal. 2. Specific heats and heats of reaction, Fuel 62 (5) (1983) 540–546. doi:10.1016/0016-2361(83)90223-5.

[38] D. Green, R. Perry, Perry's Chemical Engineers' Handbook, Eighth Edition, McGraw Hill professional, McGraw-Hill Education, 2007.

[39] A. Tenwolde, J. D. McNatt, L. Krahn, Thermal Properties of Wood and Wood Panel Products for Use in Buildings, USDA Forest Products Laboratory Report for Oak Ridge National Laboratory, Oak Ridge, TN. U.S. Department of Energy, Report ORNLISub/87- 21697/1, September. (1988) 43doi:DOE / USDA-21697/ 1.

[40] C. A. Koufopanos, N. Papayannakos, G. Maschio, A. Lucchesi, Modelling of the pyrolysis of biomass particles. Studies on kinetics, thermal and heat transfer effects, The Canadian Journal of Chemical Engineering 69 (4) (1991) 907–915. doi:10.1002/cjce.5450690413.

[41] U. S. D. o. A. F. S. Forest Products Laboratory, Wood handbook -

wood as an engineering material, General Technical Report FPL-GTR-190 (2010).

[42] C. Di Blasi, C. Branca, Kinetics of Primary Product Formation from Wood Pyrolysis, Ind. Eng. Chem. Res. 40 (23) (2001) 5547–5556. doi:10.1021/ie000997e.

[43] F. Thurner, U. Mann, Kinetic Investigation of Wood Pyrolysis, Ind. Eng. Chem. Process Des. Dev. 20 (3) (1981) 482–488.

[44] M. G. Gronli, M. C. Melaaen, M. Grønli, M. C. Melaaen, Mathematical model for wood pyrolysis - Comparison of experimental measurements with model predictions, Energy & Fuels 14 (4) (2000) 791–800. doi:10.1021/ef990176q.
URL http://pubs.acs.org/doi/abs/10.1021/ef990176q

[45] C. K. Lee, R. F. Chaiken, J. M. Singer, Charring pyrolysis of wood in fires by laser simulation, Symp. (Int.) Combust. 16 (1) (1977) 1459 –1470.

[46] J. Rath, M. G. Wolfinger, G. Steiner, G. Krammer, F. Barontini, V. Cozzani, Heat of wood pyrolysis, Fuel 82 (1) (2003) 81–91. doi:10.1016/S0016-2361(02)00138-2.

[47] L. Brown, An Experimental and Analytical Study of Wood Pyrolysis, Ph.D. thesis, University of Oklahoma (1972).

[48] B. Babu, A. Chaurasia, Pyrolysis of biomass: improved models for simultaneous kinetics and transport of heat, mass and momentum, Energ. Convers. Manage. 45 (9) (2004) 1297 – 1327.

doi:https://doi.org/10.1016/j.enconman.2003.09.013.
URL http://www.sciencedirect.com/science/article/pii/S0196890403002644

[49] Z. Duan, B. He, Y. Duan, Sphere Drag and Heat Transfer, Nature Publishing Group (2015) 1–7doi:10.1038/srep12304.
URL http://dx.doi.org/10.1038/srep12304

[50] J. M. Johansen, P. A. Jensen, P. Glarborg, N. De Martini, P. Ek, R. E. Mitchell, High Heating Rate Devolatilization Kinetics of Pulverized Biomass Fuels, Energy and Fuels 32 (12) (2018) 12955–12961. doi:10.1021/acs.energyfuels.8b03100.

[51] I. Obernberger, G. Thek, Physical characterisation and chemical composition of densified biomass fuels with regard to their combustion behaviour, Biomass and Bioenergy 27 (6) (2004) 653–669. doi:10.1016/j.biombioe.2003.07.006.

[52] H. Luo, Z. Lu, H. Wu, P. Jensen, P. Glarborg, Devolatilization of single wood particles - impact of particle density and moisture content, (unpublished results) (2018).

[53] H. Lu, Experimental and Modeling Investigations of Biomass Particle Combustion, Phd thesis, Bringham Young University (2006).

[54] N. Guo, T. Li, L. Zhao, T. Løvås, Eulerian-lagrangian simulation of pulverized biomass jet using spheroidal particle approximation, Fuel 239 (2019) 636–651.

Table 1: Model input parameters.

Parameter	**Value**	**Ref.**
h [J/(s m^2 K)]	Estimated as described by Leth-Espensen et al.	[29]
ϵ [-]	0.85	[30, 31]
$\mathcal{L}_{H_2O}$ [J/kg]	2256 000	[32]
ΔH_{desorp} [J/kg]	3610 000	[33]
ΔH_{devo} [J/kg]	200 000	[21, 34]
A_{L1} [s^{-1}]	$1.11 \cdot 10^{11}$	[9, 26]
$E_{a,L1}$ [J/mol]	$177 \cdot 10^3$	[9, 26]
A_{L2} [s^{-1}]	$9.28 \cdot 10^9$	[9, 26]
$E_{a,L2}$ [J/mol]	$149 \cdot 10^3$	[9, 26]
A_{L3} [s^{-1}]	$3.05 \cdot 10^7$	[9, 26]
$E_{a,L3}$ [J/mol]	$125 \cdot 10^3$	[9, 26]
A_H [s^{-1}]	$18.9 \cdot 10^3$	[27]
$E_{a,H}$ [J/mol]	$21.305 \cdot 10^3$	[27]
T_{boil} [K]	373.15	
C_g [J/(kg K)]	$\Big(19.50583 + 19.88705 \cdot \frac{T_g}{1000} - 8.598535 \cdot (\frac{T_g}{1000})^2 + ...$ $...1.369784 \cdot (\frac{T_g}{1000})^3 + 0.527601 \cdot (\frac{1000}{T_g})^2\Big) \cdot \frac{1000}{28}$	[35]
$C_{p,H2O\,vap}$ [J/(kg K)]	$\Big(30.09200 + 6.832514 \cdot T/1000 + 6.793435 \cdot (T/1000)^2 ...$ $...-2.53448 \cdot (T/1000)^3 + \frac{0.082139}{(T/1000)^2}\Big)\frac{1000}{18}$	[36]
$C_{p,dry\,w}$ [J/(kg K)]	$z1 = 380/T$	[37, 38]
	$z2 = 1800/T$	
	$g1 = z1^2 \cdot exp(z1)/(exp(z1) - 1)^2$	
	$g2 = z2^2 \cdot exp(z2)/(exp(z2) - 1)^2$	
	$C_{p,dry\,w} = (g1 + 2 \cdot g2) \cdot 1000 \cdot R \;/\; 7.72$	
$C_{p,wet\,w}$ [J/(kg K)]	$A = 10^3 \cdot ((0.02355T - 1.320y/(1-y) - 6.191)y/(1-y)$	[39]
	$C_{p,wet} = C_{p,wood}(1-y) + 4190y + A$	
$C_{p,char}$ [J/(kg K)]	$C_{p,char} = (g1 + 2 \cdot g2) \cdot 1000 \cdot R \;/\; 11.3$	[37, 38]
$k_{wet\,wood}$ [J/(m K s)]	$1.15 \cdot min(0.13 + 0.0003 \cdot (T - 273), 0.3)$	[28, 40, 41]
$k_{dry\,wood}$ [J/(m K s)]	$min(0.13 + 0.0003 \cdot (T - 273), 0.3)$	[28, 40]
k_{char} [J/(m K s)]	$max(0.08 - (T - 273) \cdot 10^{-8}, 0.3)$	[28, 40, 41]
Shrin. ratio drying [-]	10 % (compared to wet)	[20]
Shrin. ratio devol. [-]	50 % (compared to dry)	[20]

Table 2: Parameter intervals in which the model validation has been conducted.

Parameter	**Min**	**Max**
d_p	79 µm	9.5 mm
Moisture [wt % wb]	0	6
T_g [K]	1276	1667
ρ [kg/m^3 (dry)]	580	1000
AR [-]	1	4

Table 3: Applied model input parameters used to simulate the experiments of Johansen et al.[27] *Completely dry particles, but moisture content $>$ 0 for mathematical reasons.**Obernberger et al.[51] ***Masche et al. [13]

Parameter	T_g **= 1405 K**	T_g **= 1667 K**
h_{coef} [J/(s m^2 K)]	1881	2076
R [µm]	39.4	39.4
L*** [µm]	157.6	157.6
ρ** [kg/m^3]	591	591
T_{wall} [K] (estimated value)	1205	1467
T_{gas} [K]	1405	1667
char yield [wt% daf]	4.0	6.4
ash yield [wt% db]	0.2	0.2
Moist cont* [wt % wb]	0.0001	0.0001

Table 4: Applied model input parameters used to simulate the experiments of Lu et al.[52] *Estimated from empirical correlation from Leth-Espensen et al.,[29] determined for ρ = 600, 800, and 1000 kg/m^3.

Parameter	**Pine**	**Beech**
h_{coef} [J/(s m^2 K)]	112.0	114.2
R [mm]	1.56	1.515
T_{wall} [K] (estimated value)	1187	1187
T_{gas} [K]	1487	1487
char yield* [wt% daf]	7.6/8.1/8.5	12.8/13.6/14.2
Moist cont [wt % wb]	5.5	5.5

Table 5: Applied model input parameters used to simulate the experiments of Lu.[53]

Parameter	**Cylinder**	**Sphere**
h_{coef} [J/(s m^2 K)]	54.43	54.43
R [mm]	4.75	4.75
L [mm]	38	-
ρ [kg/m^3]	580	580
T_{wall} [K] (estimated value)	1176	1176
T_{gas} [K]	1276	1276
char yield [wt% daf]	8.4	6.4
Moist cont [wt % wb]	6	6

Table 6: Parameters for sensitivity analysis.

Parameter	**Value**
AR [-]	2
T_g [K]	1600
ρ [kg/m^3]	700
char [wt % daf]	5
moist [wt% wb]	4
ΔH_{devo} [j/kg]	200 000
ΔH_{desorp} [j/kg]	3 610 000

Table 7: Sensitivity Analysis. Each parameter is decreased and increased by 30 %. The change in devolatilization time is marked for each particle size as a percentage of the devolatilizatoin time for the particle with no change in input parameter. t_{devo} for each of the three baseline particles are also included in the table.

Parameter	**-30 %**	**+30 %**	**-30 %**	**+30 %**	**-30 %**	**+30 %**
R [μm]	**39.4**		**400**		**1560**	
t_{devo} [s]	**0.0133**		**0.426**		**3.61**	
k_p [J/(m K s)]	+5	-3	+12	-6	+29	-15
C_p [J/(kg K)]	-15	+14	-14	+13	-11	+11
h_{coef} [J/(s m^2 K)]	+23	-14	+15	-10	+4	-3
R [μm]	-35	+38	-37	+40	-41	+47
L (R constant) [μm]	-6	+3	-7	+4	-10	+6
ρ [kg/m^3]	-23	+20	-27	+26	-30	+30
T_{gas} [K]	+82	-31	+40	-21	+11	-8
k_L, k_H	+10	-7	+4	-3	+1	0
char yield [wt% daf]	-2	0	-1	0	0	0
Moist cont [wt % wb]	-2	+2	-4	+4	-4	+4
ΔH_{devo} [J/kg]	-5	+3	-2	+2	-2	+2
ΔH_{desorp} [J/kg]	-2	+2	-3	+3	-3	+3

Table 8: Overview over input parameters for particle simulation. The following values are used when nothing else is mentioned.

Parameter	**Value**
AR [-]	5
T_g [K]	1600
R [mm]	0.755
ρ [kg/m^3]	700
moist [wt% wb]	4